Wave basin testing of optimal PTO control of 6-float M4 WEC

Wave basin testing of optimal PTO control of 6-float M4 WEC

Z. Liao, T. Sun, P. Stansby & G. Li
School of Engineering, University of Manchester, Manchester, UK

M. Al-ani
Bristol Research and Innovation Laboratory, Toshiba Europe Ltd., Bristol, UK

M. Belmont
College of Engineering, University of Exeter, Exeter, UK

ABSTRACT: Power-take-off (PTO) control is applied to the multi-float attenuator-type wave energy converter (WEC) M4, with two PTOs in a 6-float configuration, and tested experimentally in a wave basin. Previous control applications using wave predictions from auto-regression (AR) and linear non-causal optimal control (LNOC) have shown average power to be increased by 30%-100% in numerical simulations. In this experiment two DC servo-motors are used to execute the control algorithm implemented on a microprocessor. Average power is calculated from the recorded torque and hinge velocity measurements. Both causal and non-causal control are applied, with deterministic sea wave prediction (DSWP) rather than AR, and a torque limit of 3 Nm, and also 6 Nm for the non-causal case. Causal control improves average power by up to 49% while non-causal (LNOC) by up to about 116% with a 3 Nm torque limit and 274% with a torque limit of 6 Nm.

1 INTRODUCTION

There has been considerable research effort on the application of control to WEC power take off to improve power capture. This has been mainly applied to heaving point absorbers, e.g. by latching (Babarit & Clément 2006), and more recently to the multi-float attenuator-type WEC M4 with one (Liao et al. 2020) or more PTOs (Liao et al. 2021) with linear non-causal optimal control (LNOC) with forward wave force prediction through auto-regression, giving mean power increases of 30-100% depending on wave period. These are purely numerical simulation results.

Wave basin test is an important way of demonstrating wave energy technologies. However, most of the conducted wave basin tests in the literatures, e.g., Stansby et al. (2017), Nicola et al. (2017), Giorgi et al. (2019), McNatt & Retzler (2020), are targeted on validating WEC models rather than applying active control strategies to improve the WEC's power capture.

Here results for the 6-float, 2-PTO WEC M4 (Carpintero Moreno & Stansby 2019), shown in figure 1, are presented, at about 1:50 scale, in irregular JONSWAP waves in the Plymouth COAST basin. The torque is controlled through two servo DC motors to optimise energy capture with causal or non-causal control. DSWP (Belmont et al. 2014) is used

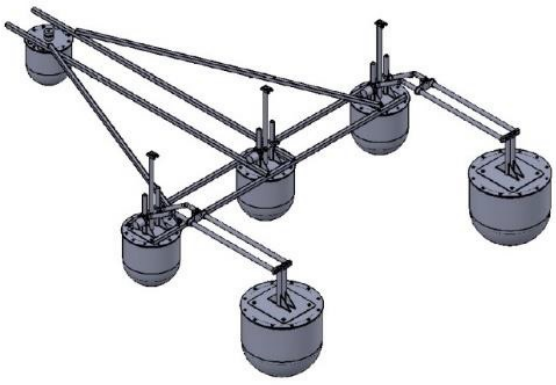

Figure 1: 6-float (1-3-2) M4 WEC (Carpintero Moreno & Stansby 2019).

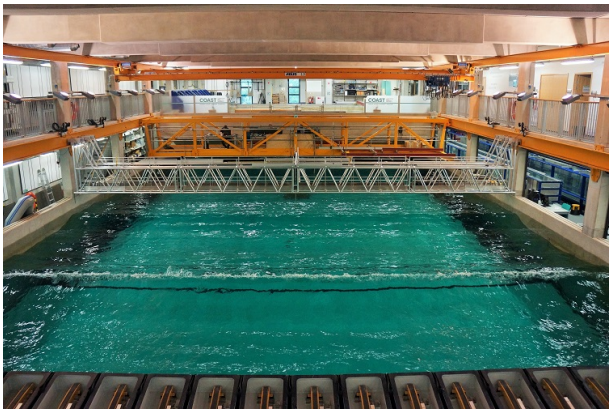

Figure 2: View of the COAST wave basin.

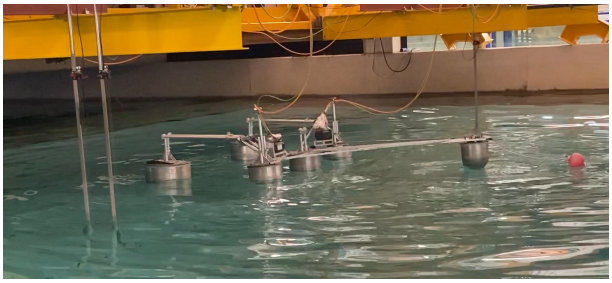

Figure 3: 6-float M4 in the COAST wave basin.

(rather than auto-regression) with LNOC, with two torque limits, 3 Nm and 6 Nm. Results show that the benefit of control is considerable and greater than predicted by purely linear diffraction-radiation modelling (Liao et al. 2020, Liao et al. 2021). With a linear damper with fixed proportional factor (passive) the mean power is relatively small, with causal control allowing this factor to vary this is improved by up to 49% with a causal or non-causal observer having little effect, with LNOC+DSWP this is increased by up to 116% with a torque limit of 3 Nm, and up to 274% with a 6 Nm torque limit. These results are surprising and encouraging. However the peak to mean power can be high, determining power quality, which is discussed for example in Karayaka et al. (2021). In due course cost functions should include this ratio as well as energy capture and incorporate machine hardware constraints more generally with multi-PTOs. This is being addressed in an ongoing project.

2 EXPERIMENTAL SET-UP

The wave basin test was carried out in the Plymouth COAST wave basin, see figure 2. The basin is 35 m long by 15.5 m wide with a movable floor allowing different operating depths. Water depth adopted in this test was 1 m. Unidirectional, irregular JONSWAP waves were generated to test the WEC with or without LNOC. There were, in total, 9 sea states labelled as IR01 to IR09. The significant wave height was fixed to 0.04 m (2 m in full scale) and the peak periods ranged from 0.8 s to 2.0 s (5.7 s to 14.1 s in full scale). Enhancement factor of the JONSWAP spectra was $\gamma = 3.3$. Each test was run for 210 seconds.

The 6-float M4 WEC has one bow float, three mid floats and two stern floats. Bow and mid floats are connected rigidly and stern floats are connected by two beams independently to the hinge point above the mid floats. When waves propagate through the WEC from bow to stern, phase difference among floats causes the device to rotate against hinge points, and thus the wave power can be transferred to mechanical power on the WEC body. Two DC servo motors are placed at the hinge points as two PTOs to provide two controlled torques for greater power capture. These motors can be controlled as passive dampers for benchmark control or as active controller, i.e. LNOC with wave predictions from DSWP. They are connected to the cabinet on the gantry through two power cables for power supply and two signal cables for communication purpose. A microprocessor is used for real-time control implementation and data processing.

The M4 WEC was moored about 15 m away from the wave paddles using a single point mooring with inextensible cables for station keeping (Stansby & Carpintero Moreno 2020). Wave gauges were deployed to measure surface elevation at different locations in the basin. One of them was placed 8 m ahead of the WEC upstream of the wave propagation direction. It is mainly for wave prediction (DSWP) purpose. The other two were placed 3 m away from the WEC on both sides for validating the actual sea state.

Experimental data are recorded by the microprocessor. A trigger signal is sent from the wave basin PC to the microprocessor when the wave paddles start generating waves so that the waves and WEC response data can be synchronised.

Figure 3 shows the WEC operating with LNOC under sea state IR02.

3 MODELLING AND OPTIMAL CONTROLLER DESIGN

3.1 *Control-oriented modelling*

In order to design optimal controllers for the M4 WEC, its dynamic model is required. In this work, a time domain linear diffraction model is built for the M4 WEC and represented in state-space form.

There are, in total, 8 degrees of freedoms (DOFs) for the 6-float M4 WEC due to the hinge constraint. They are the surge, sway, heave, roll and yaw motions of the whole body and pitch motions of the bow-mid float frame as well as those of two independent stern floats. However, wave power is mainly captured by motions in surge, heave and pitch. Thus, the problem can be simplified and only DOFs related to power capture is considered. The motion vector can be chosen as $q = [x_0\, z_0\, \theta_l\, \theta_1\, \theta_2]^\top$, where x_0 and z_0 are the surge and heave motion of the reference point, θ_l is the pitch of the bow-mid float frame and θ_1 and θ_2 are the pitch motions of two PTOs.

Based on Newton's Second Law of Motion, the equation of motion for the M4 WEC in time domain is

$$M\ddot{q}(t) = f_{e,q}(t) + f_{rd,q}(t) + f_{rs,q}(t) + f_{pto,q}(t) \quad (1)$$

where M is the 5×5 mass and inertia matrix. $f_{e,q}(t)$ is the wave excitation force, $f_{rd,q}(t)$ is the radiation damping force, $f_{rs,q}(t)$ is the hydrostatic restoring force and $f_{pto,q}(t)$ is the PTO torque. Note that mooring force is not modelled for simplification but a small stiffness term is added to the surge to prevent model drift.

The wave excitation force is independent of the WEC motion q. It can be calculated using

$$f_{e,q}(t) = Re\{\sum_{n=1}^{N} H(\omega_n)F_{ex}(\omega_n)e^{i\omega_n t}\} \quad (2)$$

where $H(\omega_n)$ is the complex wave spectrum and $F_{ex}(\omega_n)$, which can be obtained by a hydrodynamic solver WAMIT (Lee & Newman 2013), is the excitation force exerted by unit-amplitude monochromatic wave of frequency ω_n. N is the number of total frequencies considered and in this case $N = 200$. This equation is used in numerical simulations to generate wave excitation force profile. In wave basin testing, this equation is used to calculate the future excitation force based on the wave spectrum estimated by the wave prediction algorithm, i.e. DSWP.

The radiation force in time domain is modelled using Cummin's method (Cummins 1962).

$$f_{rd,q}(t) = \int_{-\infty}^{t} F_{rd}(t-\tau)\dot{q}(\tau)d\tau \quad (3)$$

where F_{rd} is a 5×5 matrix with an impulse response function (IRF) calculated using WAMIT in each entry. The length of the IRFs are approximated to be around 8 seconds. In order to derive a state-space representation, these convolutions are replaced by a state-space model. The radiation damping state-space representation can be written as:

$$\dot{z}_s = A_s z_s + B_s \dot{q}(t)$$

$$f_{rd,q}(t) = C_s z_s + D_s \dot{q}(t) \quad (4)$$

where z_s is the auxiliary state variable of the identified state-space sub-system, which has no physical meanings. The size of the state matrices A_s, B_s, C_s, D_s can be manually chosen and has a great impact on the order of the final state-space model.

The hydrostatic restoring force can be calculated using

$$f_{rs,q}(t) = Kq(t) \quad (5)$$

where K is the 5×5 hydrostatic restoring matrix. It should be noted here that the hydrodynamic coefficients were set up for the draft configuration of (Carpintero Moreno & Stansby 2019). The experimental configuration here with servo-motors was somewhat heavier giving a mid float draft 1.7 cm greater than before, equal to 18.7 cm rather than 17 cm. The hydrodynamic model thus has the correct mass distribution but only the approximate submerged geometry at mid float. However this error will be seen not to restrict control performance.

Equation (1) can now be rewritten as

$$(M + m_\infty)\ddot{q}(t) + f_{rd,q}(t) + Kq(t) = f_{e,q}(t) + f_{pto,q}(t)$$

$$\dot{z}_s = A_s z_s + B_s \dot{q}(t)$$

$$f_{rd,q}(t) = C_s z_s + D_s \dot{q}(t) \quad (6)$$

where m_∞ is the 5×5 added mass matrix.

Here, the PTO torque $f_{pto,q}$ is modelled as a passive damper for benchmark comparison.

$$f_{pto,q}(t) = \begin{bmatrix} 0 \\ 0 \\ -\tau_{pto1}(t) - \tau_{pto2}(t) \\ \tau_{pto1}(t) \\ \tau_{pto2}(t) \end{bmatrix} \quad (7)$$

The torque $\tau_{pto1} = -B_{mech}(\dot{\theta}_l - \dot{\theta}_1)$ and $\tau_{pto2} = -B_{mech}(\dot{\theta}_l - \dot{\theta}_2)$, where B_{mech} is a constant damping gain identical for each PTO and $(\dot{\theta}_l - \dot{\theta}_1)$, $(\dot{\theta}_l - \dot{\theta}_2)$ are the angular velocities of the relative pitch motions. A torque limit τ_{max} is implemented to protect the motor and the WEC.

$$\tau_{pto} = \begin{cases} -\tau_{max} & \text{for } \tau_{pto} < -\tau_{max} \\ \tau_{pto} & \text{for } -\tau_{max} \leq \tau_{pto} \leq \tau_{max} \\ \tau_{max} & \text{for } \tau_{pto} > \tau_{max} \end{cases} \quad (8)$$

With active control, τ_{pto1} and τ_{pto2} are calculated using the LNOC algorithm. By defining a new state vector $x := [q, \dot{q}, z_s]^\top$, the final state-space representation of the M4 WEC can be written as:

$$\dot{x} = Ax + B_w f_{e,q}(t) + B_u f_{pto,q}(t)$$

$$y = Cx + Du \quad (9)$$

where the system matrices are

$$A = \begin{bmatrix} 0_{5\times5} & I_{5\times5} & 0_{5\times n} \\ -(M+m_\infty)^{-1}K & -(M+m_\infty)^{-1}D_s & -(M+m_\infty)^{-1}C_s \\ 0_{n\times5} & B_s & A_s \end{bmatrix} \tag{10}$$

$$B_w = \begin{bmatrix} 0_{5\times5} \\ (M+m_\infty)^{-1} \\ 0_{n\times5} \end{bmatrix} \tag{11}$$

$$B_u = \begin{bmatrix} 0_{5\times1} \\ (M+m_\infty)^{-1}[0,0,-1,1,1]^\top \\ 0_{n\times1} \end{bmatrix} \tag{12}$$

$$C = \begin{bmatrix} 0_{1\times5} & [0\,0\,1-1\,0] & 0_{1\times n} \\ 0_{1\times5} & [0\,0\,1\,0-1] & 0_{1\times n} \end{bmatrix} \tag{13}$$

$$D = \begin{bmatrix} 0_{2\times(n+10)} \end{bmatrix} \tag{14}$$

where I is the identity matrix and 0 is matrix with zeros in all entries. The size of A depends on the selected model order n for the radiation sub-system and in this case $A \in \mathbb{R}^{210\times210}$.

3.2 *The LNOC theory*

The LNOC controller is designed based on the state-space model derived in the last section. This control framework is briefly discussed in this section, readers can refer to (Liao et al. 2019) for more details.

The LNOC algorithm is derived by solving the optimal control problem with a cost function:

$$\min_{u_0,\ldots,u_N} \Sigma_{k=0}^{N} \left\{ z_k u_k + \frac{1}{2} x_k^T Q x_k + \frac{1}{2} R u_k^2 \right\} \tag{15}$$

subject to the discrete-time version of the system equation (9):

$$x_{k+1} = Ax_k + B_w w_k + B_u u_k$$

$$z_k = Cx_k \tag{16}$$

where w_k is the 5×1 excitation force at time instant k and u_k is the PTO torque (control input). Note that here z_k is the relative pitch velocity

$$z_k = \begin{bmatrix} \dot{\theta}_l - \dot{\theta}_1 \\ \dot{\theta}_l - \dot{\theta}_2 \end{bmatrix} \tag{17}$$

The instant power absorbed by the WEC is $p_k = -z_k^\top u_k$. The first term in the cost function equation (15) is used to maximise the absorbed energy. The second and the third term are used to penalize the state and input of the control system. The weighting matrices Q and R are tunable parameters and have a huge impact on the performance of the controller.

The control policy obtained from solving the above optimal control problem has the form of:

$$u_k = K_x x_k + K_d w_{k,n_p} \tag{18}$$

Here, w_{k,n_p} is the incoming excitation force sequence $w_{k,n_p} := [w_k, w_{k+1}, \ldots, w_{k+n_p-1}]^\top$ and n_p is the length of the prediction horizon. K_x and K_d are constant control gain matrices and the formulae for calculating them are:

$$K_x = -(R + B_u^T V B_u)^{-1}(C + B_u^T V A) \tag{19}$$

$$K_d = -(R + B_u^T V B_u)^{-1} B_u^T \Psi \tag{20}$$

and

$$V = Q + A^T V A - (C + B_u^T V A)^T$$

$$(R + B_u^T V B_u)^{-1}(C + B_u^T V A) \tag{21}$$

where V is the solution of the algebraic Ricatti equation (21).

Note that the control policy equation (18) consists of two parts, which are the feedback (causal) part $K_x x_k$ and the feed-forward (non-causal) part $K_d w_{k,n_p}$. Implementing the LNOC without feed-forward part results in a causal controller, termed LOC.

On the other hand, wave prediction information is obtained by the DSWP algorithm. It takes a truncation of the latest upstream elevation measurements, computes the governing wave spectrum in the wave tank, then predicts the surface elevation at the WEC's location downstream. Readers are referred to (Belmont et al. 2014) for more details of the DSWP theory.

3.3 *Real-time implementation of the LNOC and the LOC*

Real-time implementation of controllers is accomplished by compiling and downloading cyclic tasks (written in C language) onto the microprocessor. Each cyclic task is assigned a fixed sampling time and run repeatedly. Figure 4 and figure 5 show the flow chart of LOC and LNOC, respectively. Cyclic tasks are represented by rectangle with task name inside.

The LOC is a relatively simple implementation as all the cyclic tasks are with the same 20 ms sampling time. Every 20 ms, the Data Acquisition & Processing (DAQ) task takes real-time measurements from the servo motors. These measurements are processed to obtain the hinge velocity, hinge angle and the actual torque provided by the motor. The feedback information is fed to the observer to estimate the full state information. The LOC task takes the state information and multiplied it by K_x to provide the required control signal to the motor.

The LNOC implementation is more sophisticated as it requires wave prediction algorithm DSWP. The DSWP is run at a lower frequency (500 ms) as each run can provide predictions for 2 seconds. Measurements from wave gauge is obtained by the DAQ and accumulated in a shared buffer. Every half a second

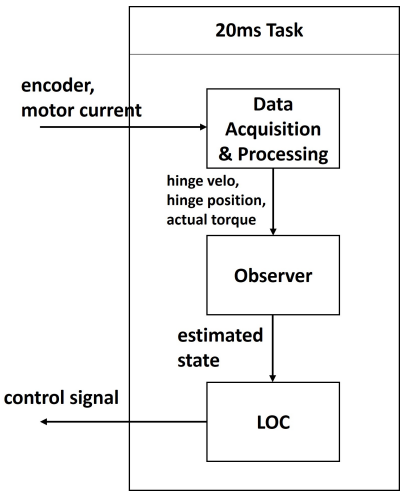

Figure 4: The LOC flow chart.

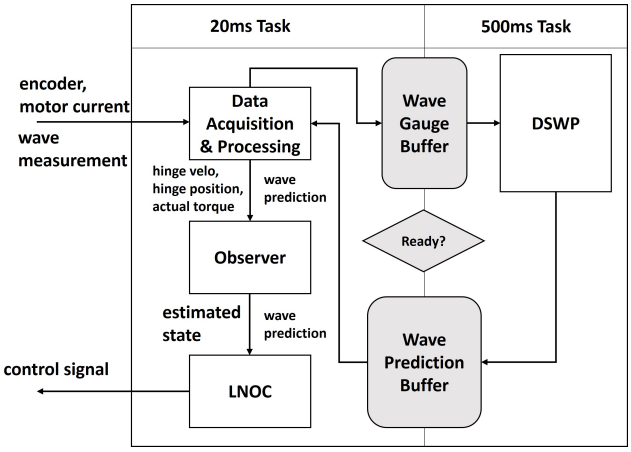

Figure 5: The LNOC flow chart.

the DSWP task takes the measurements to calculate the incoming wave prediction at the WEC's location and store the prediction into another buffer. It will also signal the DAQ task to update the wave prediction which is required by the LNOC.

Real-time codes can be re-compiled and downloaded to the microprocessor between tests so that different controllers can be tested flexibly.

4 EXPERIMENTAL RESULTS

Irregular wave tests with control were carried out in the following orders: passive damper, LOC and LNOC.

Figure 6 shows the average absorbed power for different controllers in all the tested sea states. Average power is calculated from 20 s after the trigger to allow time for the waves to reach the WEC location. Prediction horizon of the DSWP is fixed at 2 seconds. It can be noticed that the resonance peak period for the M4 WEC is near 0.9 s. Benefits of active control are obvious. With the causal controller LOC, around 50% improvement is observed at $T_p = 0.9$ s. Causal or non-causal observer have negligible effect on the controller's performance. Note that for passive damper

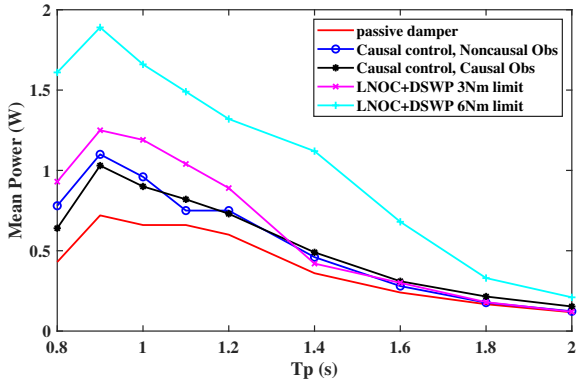

Figure 6: Mean power against peak periods.

and causal control the torque limit is 3 Nm.

With LNOC+DSWP where 2 seconds' incoming wave predictions are available, the improvement of average power is more significant. For the same PTO torque limit the percentage of improvement is up to 116%. For a larger torque limit, i.e. 6 Nm, the improvement can be up to 274%, although higher torque limit inevitably increases the cost of the PTO.

Note that for all the controllers, improvements tend to be bigger for shorter peak periods. This can be explained by the fact that the prediction horizon of DSWP is fixed due to computational capability limit of the microprocessor. Two seconds of incoming wave prediction is relatively longer for shorter peak periods. In order to completely reveal the potential of LNOC, especially for longer peak periods, a microprocessor with more powerful computational capability is required.

All the experimental data are presented in detail in Table 1. Mean power for causal and non-causal control are expressed in improvement ratio over the mean power of passive damper.

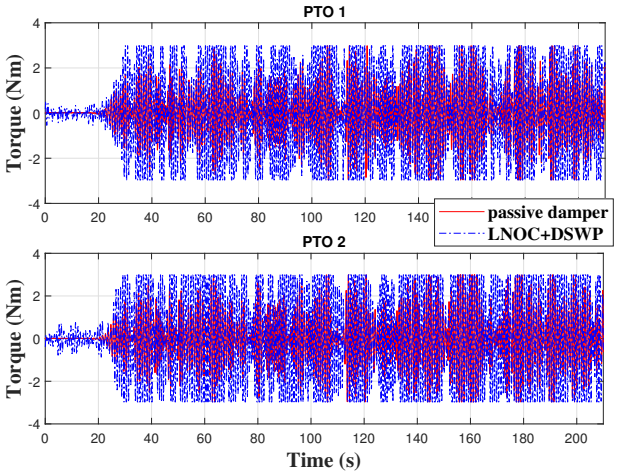

Figure 7: PTO torque (Nm) time variation (IR01, $H_s = 0.04$ m, $T_p = 0.8$ s).

Figure 7 to figure 10 show the WEC responses including PTO torques, hinge velocities, instant power and absorbed energy, comparing passive damper and LNOC+DSWP under the same torque limit (3 Nm) with sea state IR01. Each figure shows data for both of

Table 1: Experimental results of different controllers. Damper refers to the well-tuned passive damper with constant damping ratio $B_{mech} = 6$ Nms/rad. LOC stands for causal optimal control, LNOC1 stands for non-causal optimal control with 3 Nm torque limit and LNOC2 stands for non-causal optimal control with 6 Nm torque limit. Mean power is expressed as improvement ratio over passive damper for control.

Test Series	H_s [m]	T_p [s]	Mean power [W]				Peak to mean power ratio			
			Damper	LOC	LNOC1	LNOC2	Damper	LOC	LNOC1	LNOC2
IR01	0.04	0.8	0.43	49%	116%	274%	10	7	7	10
IR02	0.04	0.9	0.72	43%	74%	175%	9	6	6	9
IR03	0.04	1.0	0.66	36%	80%	152%	11	8	12	9
IR04	0.04	1.1	0.66	24%	58%	126%	12	12	10	16
IR05	0.04	1.2	0.60	22%	48%	120%	12	12	19	16
IR06	0.04	1.4	0.36	36%	17%	211%	13	13	21	22
IR07	0.04	1.6	0.24	29%	/	183%	18	15	/	31
IR08	0.04	1.8	0.17	29%	7.8%	98%	22	20	36	34
IR09	0.04	2.0	0.12	31%	/	79%	25	22	/	43

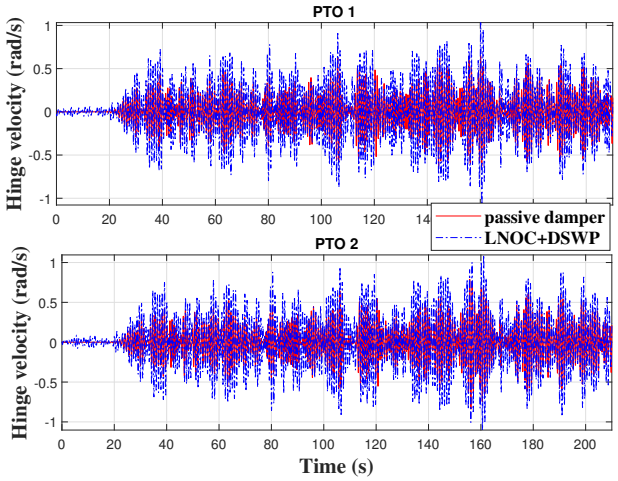

Figure 8: Hinge velocity (rad/s) time variation (IR01, $H_s = 0.04$ m, $T_p = 0.8$ s).

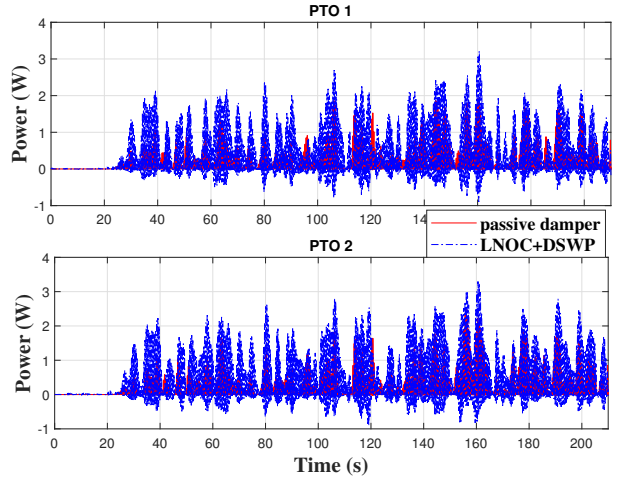

Figure 9: Absorbed power (W) time variation (IR01, $H_s = 0.04$ m, $T_p = 0.8$ s).

the two PTOs. It can be seen that with LNOC+DSWP the WEC responds more actively than with a passive damper. The root mean square (RMS) value of hinge velocity goes from 0.20 rad/s to 0.32 rad/s for PTO1 and from 0.22 rad/s to 0.35 rad/s for PTO2. For

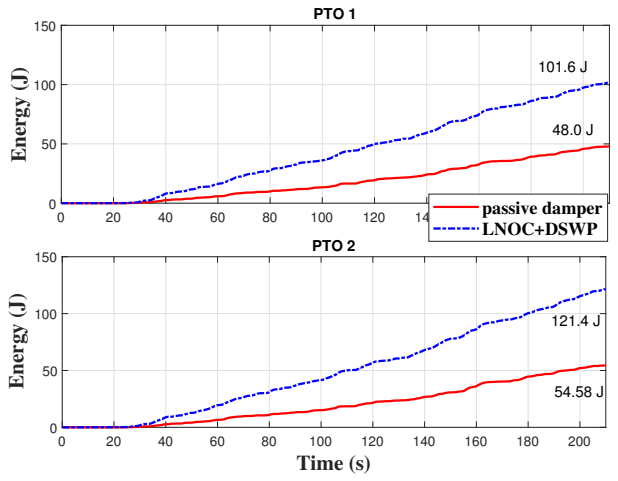

Figure 10: Absorbed energy (J) time variation (IR01, $H_s = 0.04$ m, $T_p = 0.8$ s).

LNOC+DSWP, negative power flow can occur which is expected. The improvements of average power are 110% and 117% for PTO1 and PTO2, respectively.

Interestingly, the two PTOs are not operating identically. This can be observed more clearly in figure 11 where the mean power is shown for PTO1 and PTO2,

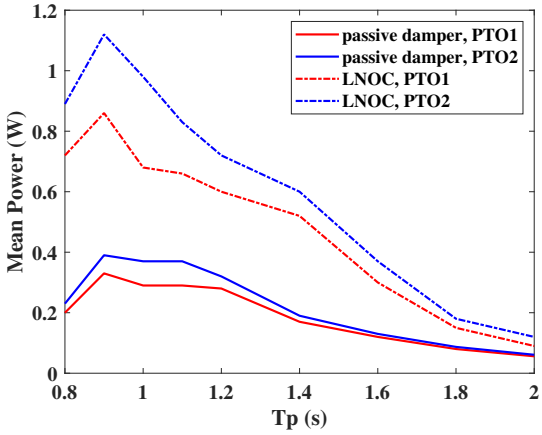

Figure 11: Comparison between between mean power (W) from two PTOs with peak period Tp (s).

with passive damper or LNOC, respectively. For either cases, PTO2 captures slightly more power than PTO1. In wave basin it is noticed that the WEC is not perfectly aligned with the wave propagating direction which may explain this. This issue can also possibly be caused by a slightly asymmetric mechanical design of the two PTOs and it will be further investigated in our future work.

5 CONCLUSIONS

Wave basin test results of PTO control for the 6-float M4 WEC are presented in this paper. Two controllable servo motors are used to provide PTO torques to the WEC hinge. Average powers are calculated to demonstrate improvements of power capture. Compared with a well-tuned passive damper, with LOC the improvement is up to 49% and with LNOC+DSWP the improvement is up to 116% with a 3 Nm torque limit and up to 274% with a 6 Nm torque limit.

These results imply that wave predictions and PTO torque limitation are two key factors determining the power conversion efficiency of WECs. In practice, a wave prediction technique such as DSWP can be implemented with a fixed cost but the PTO torque limit is a design parameter requiring cost assessment. In future work, a realistic PTO model with hardware constraints should be considered so that a more comprehensive study on the PTO including the effect of high peak to mean power ratio and the cost of PTO torque limit can be carried out.

ACKNOWLEDGEMENTS

Funding from Engineering and Physical Sciences Research Council (EPSRC) grant "EP/V040650/1, EP/V040634/1" is gratefully acknowledged

REFERENCES

Babarit, A. & A. Clément (2006). Optimal latching control of a wave energy device in regular and irregular waves. *Applied Ocean Research 28*(2), 77 – 91.

Belmont, M. et al. (2014). An examination of the feasibility of linear deterministic sea wave prediction in multidirectional seas using wave profiling radar: Theory, simulation, and sea trials. *Journal of Atmospheric and Oceanic Technology 31*, 1601–1614.

Carpintero Moreno, E. & P. Stansby (2019). The 6-float wave energy converter m4: Ocean basin tests giving capture width, response and energy yield for several sites. *Renewable and Sustainable Energy Reviews 104*, 307–318.

Cummins, W.E. (1962). The impulse response function and ship motions. *Schiffstechnik, 9, 101-109*.

Giorgi, S., J. Davidson, M. Jakobsen, M. Kramer, & J. V. Ringwood (2019). Identification of dynamic models for a wave energy converter from experimental data. *Ocean Engineering 183*, 426–436.

Karayaka, H. B., Y.-H. Yu, & E. Muljadi (2021). Investigations into balancing peak-to-average power ratio and mean power extraction for a two-body point-absorber wave energy converter. *Energies 14*(12).

Lee, C. & J. N. Newman (2013). Wamit – user manual version 7.0. In *WAMIT Inc, Chestnut Hill, Massachusetts*.

Liao, Z., N. Gai, P. Stansby, & G. Li (2019). Linear non-causal optimal control of an attenuator type wave energy converter m4. *IEEE Transactions on Sustainable Energy*, 1–1.

Liao, Z., P. Stansby, & G. Li (2020). A generic linear non-causal optimal control framework integrated with wave excitation force prediction for multi-mode wave energy converters with application to m4. *Applied Ocean Research 97*, 102056.

Liao, Z., P. Stansby, G. Li, & E. Carpintero Moreno (2021). High-capacity wave energy conversion by multi-float, multi-pto, control and prediction: Generalized state-space modelling with linear optimal control and arbitrary headings. *IEEE Transactions on Sustainable Energy 12*(4), 2123–2131.

McNatt, J. & C. Retzler (2020). The performance of the mocean m100 wave energy converter described through numerical and physical modelling. *International Marine Energy Journal 3*, 11–19.

Nicola, P., B. Giovanni, P. Biagio, S. S. Antonello, V. Giacomo, M. Giuliana, & S. Gianmaria (2017). Wave tank testing of a pendulum wave energy converter 1:12 scale model. *International Journal of Applied Mechanics 09*(02), 1750024.

Stansby, P. & E. Carpintero Moreno (2020). Hydrodynamics of the multi-float wave energy converter m4 with slack moorings: Time domain linear diffraction-radiation modelling with mean force and experimental comparison. *Applied Ocean Research 97*, 102070.

Stansby, P., E. Carpintero Moreno, & T. Stallard (2017). Large capacity multi-float configurations for the wave energy converter m4 using a time-domain linear diffraction model. *Applied Ocean Research 68*, 53 – 64.